A COMPUTATIONAL MODEL FOR SPLITTING IN LAMINATES

F. P. van der Meer and L. J. Sluys

Faculty of Civil Engineering and Geosciences, Delft University of Technology
P.O. Box 5048, 2600 GA Delft, The Netherlands
f.p.vandermeer@tudelft.nl

ABSTRACT

A computational mesoscale model for the simulation of complex failure mechanisms in laminates is presented. It is shown that conventional continuum models do not correctly capture the splitting failure mechanism inside a ply. Therefore splitting is modeled with a discontinuity in the displacement field, employing the phantom node method with a fixed crack propagation direction. A new cohesive law is applied, which allows for robust analysis of crack propagation under mixed mode conditions

1. INTRODUCTION

Failure of composite laminates generally occurs as a sequence of events, where different mechanisms, such as fiber failure, delamination, splitting and transverse matrix cracking may all occur and interact with one another prior to ultimate failure (see e.g. [1]). The present work is intended to contribute to the development of computational modeling techniques that describe a realistic representation of each of the mechanisms that may occur. A mesolevel approach is adopted, where each ply is considered a homogeneous material. For this approach, the main distinction in failure events is between failure inside a ply (intraply) and failure between the plies (interply or delamination). The intraply failure events may be subdivided into fiber failure and matrix failure. Matrix failure is the primary concern of this paper.

For intraply failure, several continuum damage models have been introduced (see e.g. [2–5]). However, the capacity of these models to capture matrix failure patterns realistically is limited [6]. Therefore, a phantom node formulation [7] for the prediction of a splitting failure mechanism is proposed. In this formulation, the split is modeled as a discontinuity in the displacement field, while its location is not restricted to the boundaries of the finite elements. A new cohesive law for mixed mode failure is applied. The propagation direction of the split is fixed, since when a split grows, it grows, by definition, parallel to the fibers. It is foreseen that, in combination with a (continuum) model for fiber failure and interface elements for delamination, this formulation for splitting allows for the modeling of complex laminate failure mechanisms.

The paper is organized as follows. In the following section, the inadequacy of continuum damage models is briefly illustrated. Next, the phantom node model is presented, along with the applied cohesive law. The superior performance of the method in comparison with continuum damage models is presented for an off-axis tensile test.

2. CONTINUUM DAMAGE

The continuum damage theory provides a rather straightforward method for the modeling of failure. In this theory, the material stiffness is decreased as strain increases beyond a certain threshold value, such that a softening relation between stress and strain is obtained. The degradation of the stiffness can be understood as the development of voids, defects or microcracks, which reduce the effective volume of the material capable of transmitting forces. Several different continuum formulations have been proposed in the specific context of fiber-composites (see e.g. [2–5]). Typically, the stiffness degradation is done in two components, one related to fiber failure and one related to matrix failure, such as

$$\sigma_1 = (1 - \omega_{\mathrm{f}})\hat{\sigma}_1 \tag{1}$$
$$\sigma_2 = (1 - \omega_{\mathrm{m}})\hat{\sigma}_2 \tag{2}$$
$$\tau_6 = (1 - \omega_{\mathrm{m}})\hat{\tau}_6 \tag{3}$$

where ω_{f} and ω_{m} are damage variables related to fiber and matrix failure, $\hat{\boldsymbol{\sigma}}$ is the effective stress (i.e. the stress in the reduced effective volume) and $\boldsymbol{\sigma}$ is the nominal stress (i.e. the averaged stress in the homogenized continuum). The effective stress is computed with the linear elastic stiffness matrix $\mathbf{D}$

$$\hat{\boldsymbol{\sigma}} = \mathbf{D}\boldsymbol{\varepsilon} \tag{4}$$

The damage variables are equal to zero until a certain failure criterion is reached. After that, the corresponding variable grows as strain increases. The maximum value $\omega_i = 1$, corresponds with complete material failure (in mode i). In our current implementation, Hashins failure criteria [8, 9] are used. A distinguishing feature of this implementation is that artificial viscosity is used to resolve the mesh dependence that is generally present when continuum models with softening behavior are applied. For more details, the reader is referred to Reference [6].

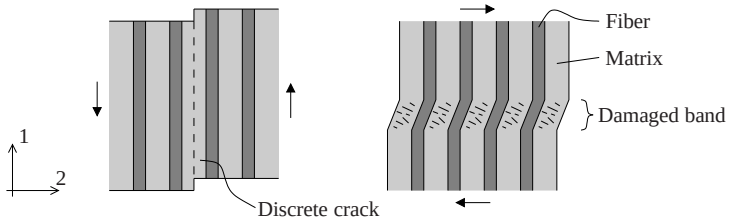

Figure 1: Localized ε_{21} corresponds to a discrete crack in the matrix or in the interface between matrix and fiber (left), while localized ε_{12} corresponds to a relatively tough failure mechanism in which a band of matrix material is damaged (right).

In [6] it is argued that the predictive quality of continuum models for failure in fiber-composites is limited. The distinction between matrix failure and fiber failure which is present in continuum damage models is not sufficient to capture the tendency of matrix cracks to grow in fiber direction. A shear band with matrix failure, which is crossed by fibers, (Figure 1 (right)), is represented with the same local stress strain behavior as a split

(Figure 1 (left)), while it is obvious from micromechanical considerations that the former is a much more ductile mechanism than the latter.
As a consequence, complex failure mechanisms, which involve splitting in single plies cannot be simulated properly when the continuum failure theorem is applied for all intraply failure mechanisms. The effects of this deficiency are clearly visibly in the simulation of the rather simple case of an off-axis tensile test on a unidirectional specimen. A single 45° ply is considered. Although failure is completely represented by matrix damage (i.e. an increase in ω_{m}), the failure band is not aligned with the fiber direction (see Figure 2).

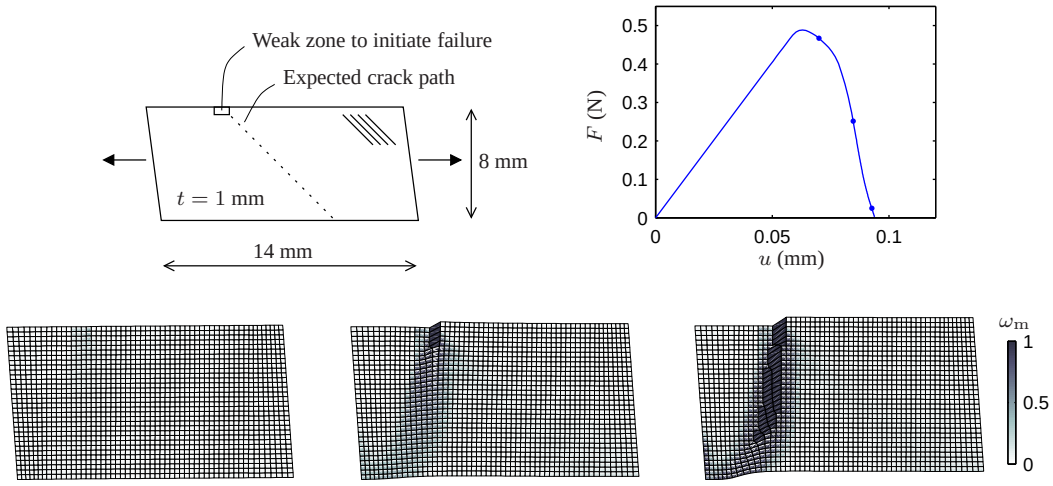

Figure 2: Off axis tensile test and results obtained with continuum damage model (deformations scaled with factor 5). The dots in the load-displacement diagram correspond with the subsequent time steps for which the deformed mesh with damage is shown.

3. PHANTOM NODE METHOD

Because of the above mentioned deficiency of continuum models, splitting should be represented in a mesoscale model for failure in laminates as a discontinuity in the displacement field. Another advantage of discontinuous models over continuum models is that the kinematics of the true phenomenon can be captured accurately with relatively large elements. One way to introduce a discontinuity in the displacement field is with the use of interface or spring elements, as has been done for splitting in [10–12]. In this work, however, the phantom node method is adopted, which has as advantages over interface elements that the crack location does not have to be known a priori and that the mesh does not have to be aligned with the crack direction.

Kinematics

Following the work by Hansbo and Hansbo [13], Mergheim et al. [14] and Song et al. [7], a crack is introduced by addition of an extra element on top of an existing element. It

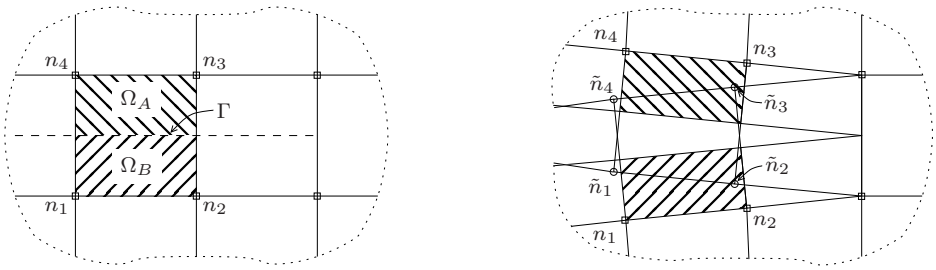

Figure 3: Representation of a discontinuity in the displacement field with the phantom node method.

has been shown [7], that this method is equivalent to the extended finite element method (XFEM) in which a discontinuity in the displacement field is introduced by enrichment of the shape functions with the Heaviside step function [15, 16].
In Figure 3, it is illustrated how the discontinuous displacement field is composed of the displacements of two overlapping elements, referred to as element A and element B. Four phantom nodes, $\tilde{n}_1, \ldots, \tilde{n}_4$, are introduced on top of the four existing nodes, $n_1, \ldots, n_4$. The element domain is subdivided by a crack segment, Γ, into subdomains Ω_A and Ω_B; Ω_A is corresponding with active part of element A and Ω_B with the active part of element B. The connectivity of the overlapping elements is

$$\begin{aligned} \text{nodes}_A &= [\tilde{n}_1, \tilde{n}_2, n_3, n_4] \\ \text{nodes}_B &= [n_1, n_2, \tilde{n}_3, \tilde{n}_4] \end{aligned} \tag{5}$$

The displacement field is defined as

$$\mathbf{u}(\mathbf{x}) = \begin{cases} \mathbf{N}(\mathbf{x})\mathbf{u}_A, & \mathbf{x} \in \Omega_A \\ \mathbf{N}(\mathbf{x})\mathbf{u}_B, & \mathbf{x} \in \Omega_B \end{cases} \tag{6}$$

where $\mathbf{N}(\mathbf{x})$ are the standard finite element shape functions and $\mathbf{u}_A$ and $\mathbf{u}_B$ are the nodal displacements of element A and element B, respectively. The displacement jump over the crack is

$$\boldsymbol{\delta}(\mathbf{x}) = \mathbf{N}(\mathbf{x}) \left(\mathbf{u}_A - \mathbf{u}_B \right), \quad \mathbf{x} \in \Gamma \tag{7}$$

Figure 3 also shows that closure of the crack tip is enforced automatically, when no phantom nodes are added on the element boundary that contains the tip.

Crack propagation

With the phantom node method, the crack tip is necessarily located on an element boundary. In crack propagation analysis, the crack may grow between the load steps, with two essential ingredients: a criterion to evaluate whether the crack should be extended and a criterion to determine the crack growth direction. For the analysis of splitting, the latter is trivial, since the propagation direction is fixed, viz. parallel to the fibers. To check whether the crack is propagating, the stress in each integration point of the element next

to the crack tip is evaluated with the Hashin criterion for tensile matrix failure in plane stress:

$$f(\boldsymbol{\sigma}) = \left(\frac{\sigma_2}{F_{2t}}\right)^2 + \left(\frac{\tau_6}{F_6}\right)^2 \leq 1 \tag{8}$$

in which F_{2t} is the transverse ply strength and F_6 is the in-plane shear ply strength. If this criterion is violated after convergence of the Newton Raphson procedure, the crack is extended through one more element, and the same load step is repeated. For crack extension, the two nodes on the element boundary that contains the old crack tip are enhanced with phantom nodes and the connectivity of the elements is adapted correspondingly.
If the criterion is satisfied in all integration points of the considered element, the converged solution is accepted, and the next load step is entered.

Bulk constitutive behavior

Linear elasticity with orthotropic stiffness is used to evaluate the bulk stress, but in principle, the phantom node method can be combined with any nonlinear material law $\boldsymbol{\sigma}(\boldsymbol{\varepsilon})$. The contribution to the nodal forces from element A is computed with

$$\mathbf{f}_A^{\text{bulk}} = \int_{\Omega_A} \mathbf{B}^T \boldsymbol{\sigma}(\boldsymbol{\varepsilon}_A)\, \mathrm{d}\Omega \quad \text{with} \quad \boldsymbol{\varepsilon}_A = \mathbf{B}\mathbf{u}_A \tag{9}$$

And similarly, the contribution to the nodal forced from element B is:

$$\mathbf{f}_B^{\text{bulk}} = \int_{\Omega_B} \mathbf{B}^T \boldsymbol{\sigma}(\boldsymbol{\varepsilon}_B)\, \mathrm{d}\Omega \quad \text{with} \quad \boldsymbol{\varepsilon}_B = \mathbf{B}\mathbf{u}_B \tag{10}$$

Cohesive traction law

A cohesive traction is applied on the crack surface. With this, the amount of energy that is dissipated as the crack propagates can be controlled and the singularity in the strain and stress field near the crack tip is avoided. Ideally, the traction $\mathbf{t}$ would be defined as a function of the displacement jump $\boldsymbol{\delta}$. However, the application of a direct traction separation law for mixed mode cracking leads to computational instability. This stems from the fact that the traction is not uniquely defined for zero crack opening; in a uniaxial case it is obvious that the traction should be equal to the strength, but in a mixed mode formulation it can be either equal to the normal strength with no shear traction, or to the shear strength with no normal traction, or something in between. The traction evaluation itself is always feasible, because after crack extension the crack opening which gives equilibrium will not be equal to zero, but the highly nonlinear nature of the traction separation law does endanger the stability of the Newton Raphson procedure.
However, the traction law may be constrained using equilibrium considerations. When the bulk element that is cut by the crack segment is dominantly loaded in tension, equilibrium demands that the traction in the crack is also dominantly tensile, and when the bulk element is loaded in shear, the traction should be shear traction. With this in mind,

a new traction law, in which the bulk stress is taken into account, has been developed by Moonen et al. [17].
Similar to continuum damage, an effective traction is computed, which can be interpreted as the effective traction working on the reduced surface of a partially cracked domain. The effective traction is defined in the local frame $\{n, s\}$:

$$\hat{\mathbf{t}} = \begin{bmatrix} \hat{t}_n \\ \hat{t}_s \end{bmatrix} = \mathbf{Q}\boldsymbol{\sigma}_\Gamma \mathbf{n} + \mathbf{T}\mathbf{Q}\boldsymbol{\delta} \tag{11}$$

where $\mathbf{T}$ is the acoustic tensor [18], which is, for orthotropic materials with $\mathbf{n}$ in transverse direction:

$$\mathbf{T} = \begin{bmatrix} \bar{D}_{22} & 0 \\ 0 & \bar{D}_{66} \end{bmatrix} \tag{12}$$

in which $\bar{\mathbf{D}}$ is the elastic stiffness matrix in the material frame. $\mathbf{Q}$ is the rotation matrix

$$\mathbf{Q} = \begin{bmatrix} -\sin\phi & \cos\phi \\ \cos\phi & \sin\phi \end{bmatrix} \tag{13}$$

in which ϕ is the angle between the crack segment and the x-axis.
In Voigt notation, $\boldsymbol{\sigma}_\Gamma \mathbf{n}$ is computed as

$$\boldsymbol{\sigma}_\Gamma \mathbf{n} = \mathbf{H}\boldsymbol{\sigma}_\Gamma \quad \text{with} \quad \mathbf{H} = \begin{bmatrix} n_x & 0 & n_y \\ 0 & n_y & n_x \end{bmatrix} \tag{14}$$

The bulk stress at Γ is not uniquely defined. We compute the stress with the averaged strain of the overlapping elements

$$\boldsymbol{\sigma}_\Gamma = \boldsymbol{\sigma}(\boldsymbol{\varepsilon}_\Gamma) \quad \text{with} \quad \boldsymbol{\varepsilon}_\Gamma = \frac{1}{2}\left(\boldsymbol{\varepsilon}_A + \boldsymbol{\varepsilon}_B\right) \tag{15}$$

Similar to continuum damage, the nominal traction is computed with

$$\mathbf{t} = (1 - \omega)\hat{\mathbf{t}} \tag{16}$$

where $\mathbf{t}$ is the nominal traction in the $\{n, s\}$-frame.
The state variable is computed with effective traction is evaluated with

$$\kappa = \sqrt{\left(\frac{\hat{t}_n}{F_{2t}}\right)^2 + \left(\frac{\hat{t}_s}{F_6}\right)^2} \tag{17}$$

Similar to continuum damage with linear softening, ω is computed with

$$\omega = \frac{\kappa^f(\kappa - 1)}{\kappa(\kappa^f - 1)} \tag{18}$$

under the loading/unloading condition $\dot{\omega} \geq 0$ and considering the limit $\omega \leq 1$. Notably,

everything goes well automatically when the first tangent after crack extension is computed with the displacement field from the previous step, for which $\boldsymbol{\delta} = 0$ and the traction is smaller than the strength. Then $\kappa < 1$ and $\omega < 0$, but the computed traction and tangent are still well defined and reasonable, in contrast with what would happen with a traction separation law that is purely based on crack opening.
The mode I fracture energy G_{Ic} is related to κ^f. After substitution of $\hat{t}_s = 0$ in Equation (16), a linear relation between δ_n and t_n is obtained, under the assumption that the following equilibrium relation holds

$$t_n = (\mathbf{QH}\boldsymbol{\sigma})_n, \quad t_s = (\mathbf{QH}\boldsymbol{\sigma})_s \tag{19}$$

Subsequently, with

$$G_{Ic} = \int_0^\infty t_n \, \mathrm{d}\delta_n \tag{20}$$

κ_f may be expressed in terms of material parameters G_{Ic} and F_{2t}:

$$\kappa^f = \frac{2G_{Ic}\bar{D}_{22}}{F_{2t}^2} \tag{21}$$

In the current formulation, the mode II fracture energy is a dependent quantity:

$$G_{IIc} = \frac{G_{Ic}\bar{D}_{22}F_6^2}{\bar{D}_{66}F_{2t}^2} \tag{22}$$

The contribution to the nodal forces from the cohesive traction are computed with

$$\mathbf{f}_A^{\mathrm{coh}} = -\mathbf{f}_B^{\mathrm{coh}} = \int_\Gamma \mathbf{N}^T\mathbf{Q}^T\mathbf{t} \, \mathrm{d}\Gamma \tag{23}$$

Consistent linearization

The contribution to the stiffness matrix from the two overlapping elements is

$$\begin{bmatrix} \mathbf{K}_{AA} & \mathbf{K}_{AB} \\ \mathbf{K}_{BA} & \mathbf{K}_{BB} \end{bmatrix} = \begin{bmatrix} \mathbf{K}_A^{\mathrm{bulk}} & 0 \\ 0 & \mathbf{K}_B^{\mathrm{bulk}} \end{bmatrix} + \begin{bmatrix} \mathbf{K}_\delta^{\mathrm{coh}} & -\mathbf{K}_\delta^{\mathrm{coh}} \\ -\mathbf{K}_\delta^{\mathrm{coh}} & \mathbf{K}_\delta^{\mathrm{coh}} \end{bmatrix} + \begin{bmatrix} \mathbf{K}_\sigma^{\mathrm{coh}} & \mathbf{K}_\sigma^{\mathrm{coh}} \\ -\mathbf{K}_\sigma^{\mathrm{coh}} & -\mathbf{K}_\sigma^{\mathrm{coh}} \end{bmatrix} \tag{24}$$

with

$$\mathbf{K}_A^{\mathrm{bulk}} = \int_{\Omega_A} \mathbf{B}^T\mathbf{D}\mathbf{B} \, \mathrm{d}\Omega \tag{25}$$

$$\mathbf{K}_B^{\mathrm{bulk}} = \int_{\Omega_B} \mathbf{B}^T\mathbf{D}\mathbf{B} \, \mathrm{d}\Omega \tag{26}$$

$$\mathbf{K}_{\delta}^{\mathrm{coh}} = \int_{\Gamma} \mathbf{N}^T \mathbf{Q}^T \mathbf{A} \mathbf{T} \mathbf{Q} \mathbf{N} \, \mathrm{d}\Gamma \tag{27}$$

$$\mathbf{K}_{\sigma}^{\mathrm{coh}} = \frac{1}{2} \int_{\Gamma} \mathbf{N}^T \mathbf{Q}^T \mathbf{A} \mathbf{Q} \mathbf{H} \mathbf{D} \mathbf{B} \, \mathrm{d}\Gamma \tag{28}$$

The nonlinearity of the system is in matrix $\mathbf{A}$, which is defined as

$$A_{ij} = \frac{\partial t_i}{\partial \hat{t}_j} = (1-\omega)\delta_{ij} - t_i \frac{\partial \omega}{\partial \hat{t}_j}, \qquad i,j = n,s \tag{29}$$

with

$$\frac{\partial \omega}{\partial \hat{t}_j} = \frac{\partial \omega}{\partial \kappa} \frac{\partial \kappa}{\partial \hat{t}_j} \tag{30}$$

and from Eqs. (17) and (18):

$$\frac{\partial \omega}{\partial \kappa} = \frac{\kappa^f}{\kappa^2(\kappa^f - 1)} \tag{31}$$

$$\frac{\partial \kappa}{\partial \hat{t}_n} = \frac{\hat{t}_n}{\kappa F_{2t}^2} \tag{32}$$

$$\frac{\partial \kappa}{\partial \hat{t}_s} = \frac{\hat{t}_s}{\kappa F_{6}^2} \tag{33}$$

Results

The phantom node method and the presented traction law provide a framework for simulation of split propagation in laminates. Now, we revisit the 45° off-axis tensile test from Figure 2. The load displacement behavior and the deformed mesh from different stages as obtained with the phantom node method is shown in Figure 4. Contrary to the analysis discussed in Section 2., the crack grows in the correct direction, not surprisingly since the growth direction is fixed. Excellent convergence is achieved because the crack propagation is executed outside of the Newton-Raphson loop. A jump is observed in the load displacement graph at the point where the crack (the mathematical tip [16]) reaches the opposite boundary. A second jump is observed when the of the crack becomes traction free. At the end of the analysis, the load is equal to zero, which is when the traction free zone (the physical tip [16]) reaches the opposite boundary.

4. CONCLUSIONS

A method is presented for the modeling of a splitting mechanism in laminates under mixed mode conditions. The split is represented by a discontinuity in the displacement field. A cohesive traction law is implemented, which has three material parameters: transverse tensile strength, in-plane shear strength, and fracture energy related to matrix failure of the ply.

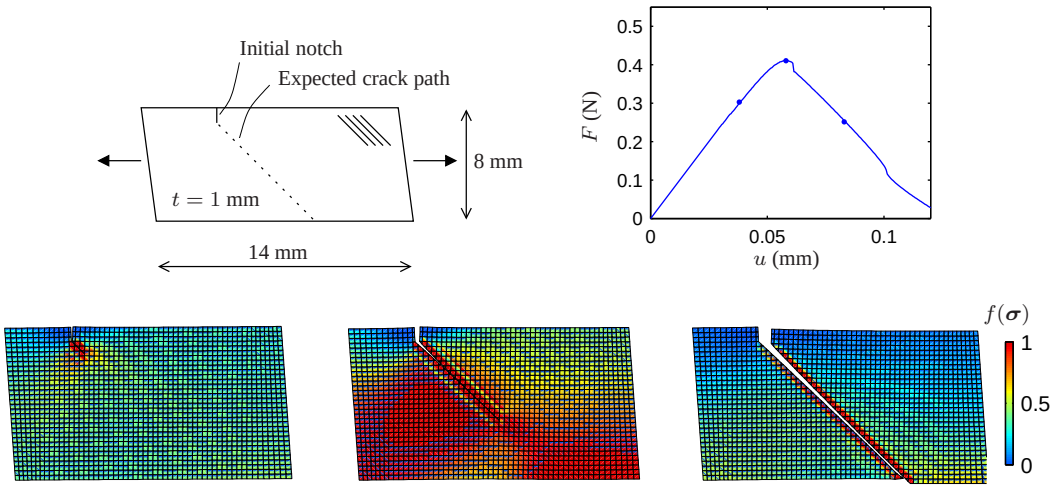

Figure 4: Mixed mode results (deformations scaled with a factor 10). The dots in the load-displacement diagram correspond with the subsequent time steps for which the deformed mesh with equivalent matrix stress (see Eq. (8)) is shown.

The crack propagation direction is set equal to the fiber direction. Therefore, the correct crack pattern is obtained, in contrast with continuum failure models, in which the tendency of cracks to grow in fiber direction is partially lost in the homogenization that is involved.

ACKNOWLEDGMENTS

This research is supported by the Technology Foundation STW (under grant DCB.6623) and the Ministry of Public Works and Water Management, The Netherlands.

REFERENCES

[1] Green, B.G., Wisnom, M.R. and Hallett, S.R. (2007). An experimental investigation into the tensile strength scaling of notched composites. *Composites: Part A*, 38: 867–878.

[2] Matzenmiller, A., Lubliner, J. and Taylor, R.L. (1995). A constitutive model for anisotropic damage in fiber-composites. *Mechanics of Materials*, 20: 125–152.

[3] Maimí, P., Camanho, P.P., Mayugo, J.A. and Dávila, C.G. (2007). A continuum damage model for composite laminates: Part I – Constitutive model. *Mechanics of Materials*, 39: 897–908.

[4] Lapczyk, I. and Hurtado, J.A. (2007). Progressive damage modeling in fiber-reinforced materials. *Composites: Part A*, 38: 2333–2341.

[5] Laš, V. and Zemčik, R. (2008). Progressive damage of unidirectional composite panels. *Journal of Composite Materials*, 42: 25–44.

[6] Meer, F.P. van der, and Sluys, L.J. (*submitted*). Continuum models for the analysis of progressive failure in composite laminates. *Journal of Composite Materials*.

[7] Song, J.H., Areias, P.M.A. and Belytschko, T. (2006). A method for dynamic crack and shear band propagation with phantom nodes. *International Journal for Numerical Methods in Engineering*, 67: 868–893.

[8] Hashin, Z. and Rotem, A. (1973). A fatigue failure criterion for fiber reinforced materials. *Journal of Composite Materials*, 7: 448–464.

[9] Hashin, Z. (1980). Failure criteria for unidirectional fiber composites. *Journal of Applied Mechanics*, 47: 329–334.

[10] Wisnom, M.R. and Chang, F.K. (2000). Modelling of splitting and delamination in notched cross-ply laminates. *Composites Science and Technology*, 60: 2849–2856.

[11] Yang, Q.D. and Cox, B.N. (2005). Cohesive models for damage evolution in laminated composites. *International Journal of Fracture*, 133: 107–137.

[12] Jiang, W.G., Hallett, S.R., Green, B.G. and Wisnom, M.R. (2007). A concise interface constitutive law for analysis of delamination and splitting in composite materials and its application to scaled notched tensile specimens. *International Journal for Numerical Methods in Engineering*, 69: 1982–1995.

[13] Hansbo, A. and Hansbo, P. (2004). A finite element method for the simulation of strong and weak discontinuities in solid mechanics. *Computer Methods in Applied Mechanics and Engineering*, 193: 3523–3540.

[14] Mergheim, J., Kuhl, E. and Steinmann, P. (2005). A finite element method for the computational modelling of cohesive cracks. *International Journal for Numerical Methods in Engineering*, 63: 276–289.

[15] Wells, G.N. and Sluys, L.J. (2001). A new method for modelling cohesive cracks using finite elements. *International Journal for Numerical Methods in Engineering*, 50: 2667–2682.

[16] Moës, N. and Belytschko, T. (2002). Extended finite element method for cohesive crack growth. *Engineering Fracture Mechanics*, 69: 813–833.

[17] Moonen, P., Sluys, L.J. and Carmeliet, J. (2007). Modeling the hygro-mechanical response of quasi-brittle materials. In A. Carpinteri et al.., editor, *Fracture Mechanics of Concrete and Concrete Sructures, Volume 1*. Taylor & Francis: London.

[18] Oliver, J. (2000). On the discrete constitutive models induced by strong discontinuity kinematics and continuum constitutive equations. *International Journal of Solids and Structures*, 37: 7207–7229.